Magnetic properties of devicelike cobalt/2D materials interfaces

Jacko Rastikian,[1] Stéphan Suffit,[1] Clément Barraud,[1] Amandine Bellec,[1] Vincent Repain,[1] Yves Roussigné,[2] Mohamed Belmeguenai,[2] Samir Farhat,[2] Ludovic Le Laurent,[3] Cyrille Barreteau,[3] and Salim Mourad Chérif[2,*]

[1]*Matériaux et Phénomènes Quantiques, Université de Paris, CNRS UMR 7162, 10, rue A. Domon et L. Duquet, 75013 Paris, France*

[2]*Laboratoire des Sciences des Procédés et des Matériaux, CNRS, LSPM UPR 3407, Université Sorbonne Paris Nord, Villetaneuse, 93430, France*

[3]*SPEC, CEA, CNRS, Université Paris-Saclay, CEA Saclay, 91191 Cedex Gif-sur-Yvette, France*

(Received 7 October 2020; revised 17 November 2020; accepted 15 December 2020; published 19 January 2021)

We have studied the magnetism of a cobalt ultrathin film deposited on different two-dimensional (2D) materials, namely graphene, h-BN, and WSe_2 by the Brillouin light scattering technique. The studied samples are prepared by a pick-up method of large flakes deposited on SiO_2 and the subsequent physical vapor deposition of metal layers, in a similar way to what is done to make spintronic devices out of such materials. Compared to the reference layer (Co/SiO_2), the perpendicular magnetic anisotropy is enhanced in the Co/2D systems, although less than what could be expected on single crystal samples. This result is quantitatively discussed by comparison with *ab initio* calculations in the case of the Co/graphene interface. We also measure an increase of the magnetic damping and a small Dzyaloshinskii-Moriya interaction in such samples which are discussed with respect to the recent literature.

DOI: 10.1103/PhysRevMaterials.5.014004

I. INTRODUCTION

Two-dimensional (2D) materials have been largely studied in the last decade due to their extraordinary electronic and optoelectronic properties [1]. More recently, it has been proposed that they can display interesting properties for spintronics. For example, graphene (Gr), with its high electronic mobility and low spin-orbit coupling, is among the best candidate for long spin diffusion lengths [2,3]. Hexagonal boron nitride (h-BN), which is a natural substrate for graphene due to a large band gap and a small lattice mismatch, also seems to have potential interest (tunnel barrier, strong spin polarization, half-metallicity) [4]. Dichalcogenides, and especially those with heavy atoms like WSe_2 have also attracted considerable attention for either spin-orbitronics [5] or light-controled spin transport [6].

Although the latter studies generally require interfaces between 2D materials and magnetic electrodes, such as cobalt, the characterization of magnetic properties in such systems is still scarce, especially in devicelike samples where the magnetic electrode is deposited on top of the 2D material before or after lithographic processes in a clean room. However, it is of high importance to know how key parameters for spintronics such as perpendicular magnetic anisotropy (PMA), magnetic damping or the Dzyaloshinskii-Moriya interaction (DMI) vary at Co/2D interfaces. Model studies on single crystals have already shown that the hybridization with the π electrons of either C_{60} [7] or graphene [8–10] could increase significantly the PMA of Co films. However, in this latter case, the Co is grown below the graphene layer by intercalation and the role of the metallic substrate could also be important to explain the PMA [11]. Theoretically, several works have predicted PMA at ferromagnet/2D interfaces [12]. Concerning DMI, the situation is quite controversial. While a significant DMI has been deduced from Gr/Co/Pt and Gr/Co/Ru single crystal samples (once again grown by intercalation where the role of the substrate is not negligible) [13,14], a recent study has shown almost no DMI for magnetic films deposited directly on pristine graphene and that induced defects in the graphene layer are necessary to obtain significant DMI [15].

In the idea of testing the potential of ferromagnetic (FM)/2D materials systems in the development of the next generation of spintronic devices, the study of the behavior of those parameters (PMA, DMI, and damping) is of great importance. An efficient approach allowing their simultaneous investigation directly on a device setup, i.e., with tens of micrometers size, is to study their dynamic magnetic properties with the Brillouin light scattering (BLS) technique. BLS is a well-known optical noninvasive tool based on the study of the spin waves (SWs) propagating within the investigated magnetic layers. As explained in the following, such an experimental approach allows one to access simultaneously perpendicular magnetic anisotropy, damping, and DMI on different hybrid FM/2D materials. More precisely, we report BLS measurements conducted on three systems, namely a thin 1.5 nm cobalt layer deposited on graphene, h-BN and WSe_2 flakes, which are compared to a Co/SiO_2 reference layer.

II. SAMPLES AND EXPERIMENTS

The studied samples are constituted of multilayer flakes of graphene, h-BN or WSe_2 deposited on a SiO_2(100 nm)/Si substrate, and subsequently covered with a thin Co film of nominal thickness of 1.5 nm, calibrated with an *in situ* quartz

*cherif@univ-paris13.fr

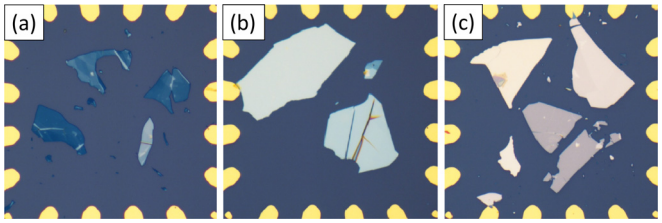

FIG. 1. $100 \times 100\ \mu m^2$ optical microscope images of the three different samples. In all cases, the chosen flakes have been deposited on SiO_2 at the center of converging gold electrodes (seen in yellow at the border of the images). The whole structure have been covered with 1.5 nm of Co and 4 nm of Au. (a) Graphene flakes. (b) h-BN flakes. (c) WSe_2 flakes.

microbalance. 100 μm scale optical microscope images of the three samples are presented in Fig. 1. The thickness of the dielectric seed material SiO_2 was chosen in order to maximize the intensity of the inelastic Brillouin scattered light signal [16]. Indeed such a boost-up of the signal eases the magnon visualization in ultrathin magnetic films, speeds-up the measurement, and increases the reliability of the data. The multilayers flakes are obtained from a standard exfoliation process from high-quality bulk crystals purchased from HQ-Graphene [1]. The 2D crystals are exfoliated and transferred over a first SiO_2(280 nm)/Si substrate. This oxide thickness is known to maximize the contrast between the randomly dispersed 2D flakes allowing a clear distinction between the different thicknesses through a specific color gradient [17,18]. The chosen multilayer flakes are of around 30 nm in thickness and of $30 \times 20\ \mu m^2$ in area. They are then selectively transferred over a prepatterened SiO_2(100 nm)/Si substrate using a dry pick-up transfer technique [19]. This transfer technique is based on the glass transition properties of polypropylene carbonate (PPC) polymer. PPC is hard and glassy at room temperature, and becomes viscous and rubbery around 40 °C and even a more fluid liquid when the temperature is raised around 70 °C. This allows a two-step process for picking-up the desired 2D flake and dropping it down precisely over a predefined area. This area is an almost 100 μm wide SiO_2 area surrounded by gold electrodes. Whereas those electrodes are generally used to connect electrically the samples with further lithographic processes, here we take advantage of such a pattern to locate easily the flakes. In BLS experiments, the gold electrodes (and the flakes to a lesser extent) diffract the focused laser beam, which allows to locate them unambiguously. The sample is finally rinsed in acetone and isopropanol for few minutes to remove polymer residues. It is then directly transferred in the evaporation chamber where we evaporate the 1.5-nm Co ultrathin film capped by a protective 4- nm-thick Au film using an electron-beam at very low rates (0.01 nm/s) in a 10^{-7} mbar range vacuum. The choice of Au as a capping layer is motivated by the vanishingly small DMI induced at the Au/Co interface [20]. During the whole fabrication process, the sample is kept in a clean-room controlled atmosphere to prevent any dust contamination.

In the BLS experiments, the sample is illuminated with a laser having a wavelength $\lambda = 532$ nm, through a lens which serves to focus the beam on a diameter $\approx 20\ \mu$m, enough to focus the light only on a single flake. The interaction of the incident beam (photons) with SW (magnons) results, for part of the backscattered photons, by a change in frequency. This scattering is the inelastic light signal. The backscattered beam is sent inside a tandem Fabry-Perot spectrometer and the signal is collected as an intensity spectrum versus the scanned frequency. The SWs with in-plane wave number k in the range 0–20 μm^{-1} are probed in the Damon-Eshbach geometry (field applied in the plane of the sample, perpendicular to the incident light), which allows SW propagating along the in-plane direction perpendicular to the applied field to be probed. After setting accurately the zero frequency shift position [21], the Stokes (f_S) and anti-Stokes (f_{AS}) frequency shifts were detected simultaneously. The SW frequencies shifts and the full width at half maximum (FWHM) were determined from the Lorentzian fits of the BLS spectra, allowing an accurate study of the perpendicular anisotropy, damping and DMI behaviours. It should be noted that the uncertainty due to finite angle of acceptance is negligible in our experiments: It corresponds to a maximal frequency uncertainty of about 3×10^{-4} GHz to be compared with the observed linewidths of about 3 GHz.

III. RESULTS

A. Perpendicular magnetic anisotropy

Figure 2 shows typical BLS spectra (in grey) with their fit (in blue) obtained for an applied field $\mu_0 H = 0.3$ T and a wave number $k = 11.8\ \mu m^{-1}$ respectively on (a) Au(4 nm)/Co(1.5 nm)/Graphene, (b) Au(4 nm)/Co(1.5 nm)/h-BN, and (c) Au(4 nm)/Co(1.5 nm)/WSe_2. For the sake of comparison, we have added as a black curve the fit of BLS spectrum recorded on the reference sample Au(4 nm)/Co(1.5 nm)/SiO_2. The first point to note is that we observe clear SW modes, typical of continuous films, indicating that even for such a small thickness the cobalt is fully covering the substrate whatever its nature.

For Co deposited on graphene, h-BN, and WSe_2, one can observe a systematic diminution of the frequency with comparison to the reference layer deposited on SiO_2. This can be attributed to an enhancement of the perpendicular magnetic anisotropy assuming that the saturation magnetization is not modified with respect to the reference layer. Indeed, naturally, the saturation magnetization can vary with the thickness of the ferromagnetic film. However, in the case of thin cobalt films, such a variation occurs mainly for thicknesses less than 1 nm as shown in Pt/Co/Pt films with Co layer thickness ranging between 0.5 and 0.8 nm [22], whereas the magnetization tends towards the value at saturation for thicknesses as low as 1.2 nm as reported in Pt/Co/AlOx films with thickness in the range 0.6–1.2 nm [23]. Mean anisotropy constants have been extracted from ferromagnetic resonance measurements of cobalt samples, down to 1.13 nm, by fitting the experimental results with a saturation magnetization equal to the bulk value [24]. We can thus infer that a 1.5-nm-thick Co layer should present a saturation magnetization similar to the bulk one.

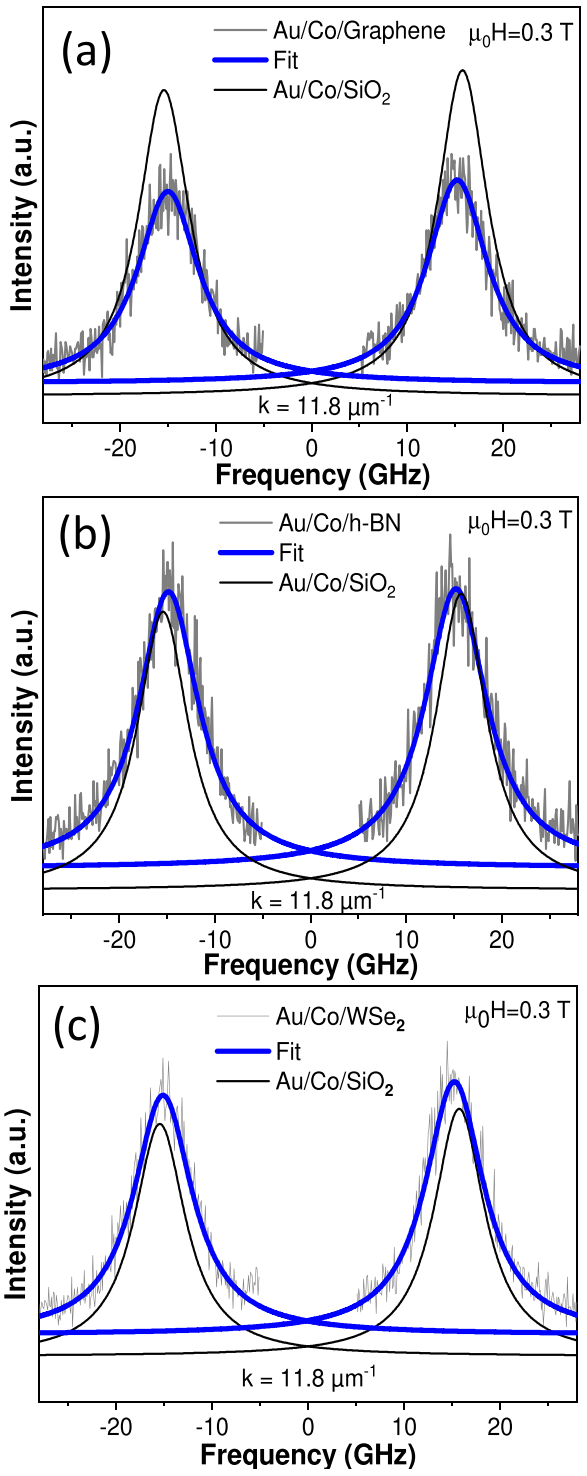

FIG. 2. BLS spectra of the reference Co sample and the (a) Co/Gr, (b) Co/h-BN and (c) Co/WSe_2 samples, for an applied magnetic field $\mu_0 H = 0.3\,T$ and a wave number $k = 11.8\,\mu m^{-1}$.

In order to quantify the changes of the magnetic properties induced by the presence of the 2D materials, we have performed BLS spectra as function of magnetic field. Indeed, we can derive a formula providing explicit expressions for the SW frequency f of the magnon lines as function of field,

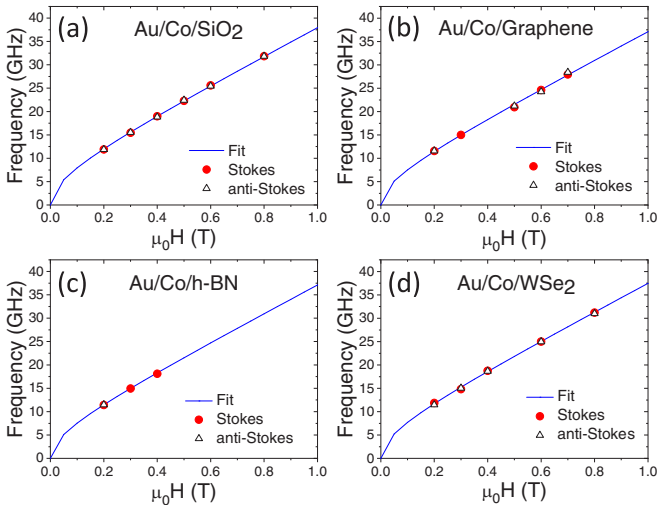

FIG. 3. Variation of the frequency as function of the applied magnetic field for (a) Co/Graphene (b) Co/h-BN, (c) Co/WSe_2, and (d) the reference Co film. Symbols are the experimental data and continuous lines represent the theoretical fit. Error bars are less than the symbol size.

depending on the magnetic anisotropy value [21]:

$$f = \frac{\gamma}{2\pi}\mu_0\sqrt{H(H + M - H_a)}, \tag{1}$$

where γ is the gyromagnetic factor, H is the external magnetic field, M is the magnetization, and $H_a = \frac{2K}{\mu_0 M}$ is the anisotropy field derived from the anisotropy energy K. Interestingly, for large applied fields, the frequency variation is linear:

$$f = \frac{\gamma}{2\pi}\mu_0\left(H + \frac{1}{2}(M - H_a)\right). \tag{2}$$

Figure 3 represents the frequency variation as function of the applied field for (a) the reference sample Au(4 nm)/Co(1.5 nm)SiO_2, (b) Au(4 nm)/Co(1.5 nm)/graphene, (c) Au(4 nm)/Co(1.5 nm)/h-BN, and (d) Au(4 nm)/Co(1.5nm)/WSe_2. The symbols are the experimental data and the continuous lines are the theoretical fit from expression (2) with $\frac{\gamma}{2\pi}$=30 GHz/T, which allows for determining the effective magnetization $\mu_0(M - H_a)$ and hence the perpendicular magnetic anisotropy.

The results are summarized in the Table I. This effective magnetization is found to be reduced in the Co/2D systems regarding to the reference sample meaning that the anisotropy field is higher in the presence of the 2D materials. However, those variations remain rather weak, about a few tens of mT. The amplitude of these perpendicular magnetic anisotropy

TABLE I. Parameters obtained from the fit of the data of Fig. 3 with the expression (2).

Sample	$\mu_0(M - H_a)$ (mT)	K (kJ/m^3)
Co/SiO_2	600	−420
Co/Gr	550	−385
Co/h-BN	530	−370
Co/WSe_2	560	−390

variations on 2D materials will be discussed with comparison to the literature in Sec. IV. It is worth noticing that discriminating the volume from the surface anisotropy requires us to study the evolution of the anisotropy as function of the thickness of the magnetic film. Indeed the perpendicular uniaxial magnetic anisotropy constant K obeys $K = K_v + K_s/t_{Co}$ where K_v is the volume contribution, K_s is the surface contribution, and t_{Co} is the Co thickness. When the effective magnetization decreases linearly with the inverse of the ferromagnetic film thickness $1/t_{Co}$, this suggests the existence of perpendicular interface anisotropy.

B. Damping

Another modification can be observed from BLS spectra related to the FWHM of the BLS lines, which increases in the presence of graphene, h-BN, and WSe_2, regarding to the reference Co film. This means that damping increases in presence of the 2D materials. For a FM material interfaced with a non-magnetic metal having a high spin orbit coupling (SOC), enhancement of the damping is usually attributed to interfacial spin pumping contribution [25]. The stronger the SOC, the higher the damping. The total damping is thus given by $\alpha = \alpha_{\mathrm{FM}} + \alpha_{\mathrm{pump}}$, where α_{FM} is the Gilbert damping of the FM and α_{pump} is the damping introduced by the spin pumping effect due to the metallic capping layer. Here we find that this mechanism is negligible, which seems reasonable as graphene is a low SOC material and h-BN and WSe_2 are nonconductive. The damping is therefore more likely due to a change in the Co film structure and morphology induced by the growth on 2D materials. Indeed, sample imperfections such as grain boundaries and grain size distribution induce inhomogeneous broadening characterized by a term added to the one due to the effective Gilbert damping [26].

In such a case, the FWHM of the BLS lines reads (cf. Supplemental Material [21]):

$$\delta f = \alpha f + \frac{\gamma}{4\pi}\mu_0 \delta H_a, \tag{3}$$

where α is the Gilbert factor and δH_a is the amplitude of anisotropy field heterogeneity. Combined with Eq. (1), one obtains the expected variation of δf with the applied field.

The experimental variation of the FWHM as function of the applied field is exhibited in Fig. 4. No clear variation is observed meaning that the enhancement of damping is mainly due to inhomogeneous broadening induced by sample imperfections in the Co/2D investigated systems, confirming that the interface induced structural quality of the Co film is a striking parameter. Note that we can estimate an upper limit of α around 10^{-2}, in agreement with the value range (0.005–0.0085) reported for hcp and fcc Co [27].

The mean value of $\mu_0 \delta H_a$ varies significantly depending on the substrate nature, from 220 mT for Co/SiO_2 to 280, 270 and 240 mT, respectively, for Co/Gr, Co/h-BN and Co/WSe_2.

C. Dzyalonshinskii-Moriya interaction

The BLS technique has proved in the last years to be a direct and robust tool for measurement of DMI constants through frequency shifts of oppositely propagating SWs

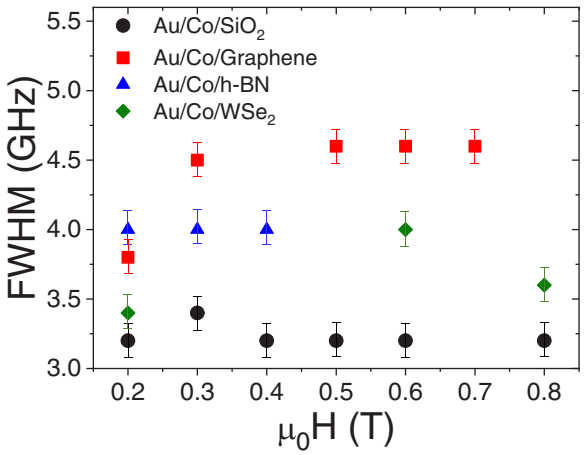

FIG. 4. FWHM of the BLS lines as function of the applied magnetic field for the reference sample Co/SiO_2 (squares), Co/Graphene (disks), Co/h-BN (triangles) and Co/WSe_2 (diamonds).

[23,28]. The frequency difference between Stokes and anti-Stokes frequencies $\Delta f = f_S - f_{\mathrm{AS}}$ gives direct information on the DMI value using $\Delta f = 2(\gamma/\pi M)D_{\mathrm{eff}}k$ [29], where γ is the gyromagnetic coefficient ($\gamma/2\pi = 30$ GHz/T and the saturation magnetization of cobalt $\mu_0 M = 1.76$ T).

Figure 5 shows BLS spectra for the Co/Gr, Co/h-BN and Co/WSe_2 samples. They were taken for a wave number $k = 20\ \mu\mathrm{m}^{-1}$ corresponding to incidence angle $\theta = 60$ deg ($k = 4\pi \sin\theta/\lambda$), the highest available value in our BLS setup, under an applied field $\mu_0 H = 0.2$ T. Importantly, mirror-symmetrical results were obtained for $\mu_0 H = -0.2$ T, as expected from nonreciprocity. From the Lorentzian fits of the spectra, Δf was estimated to be about 0.2 GHz, whatever the sample. It is important to note that the reference sample Co/SiO_2 displays perfectly symetric Stokes and anti-Stokes frequencies. Using the values of k, M, and $\gamma/2\pi$ mentioned above, we obtain D_{eff} around 0.1 mJ/m^2, a value typically ten times smaller than in $Al_2O_3/Co/Pt$ samples of similar thickness [23]. The studied 2D materials therefore induce a weak DMI, certainly of interfacial origin. Surprisingly, the presence of the heavy W atom in WSe_2 has no significant impact on the DMI value, which can be explained by the fact that W is not in direct contact with Co.

IV. DISCUSSION

A. Magnetic anisotropy

As shown in Sec. III A, the modification of magnetic anisotropy induced by the graphene substrate, as compared to SiO_2 is 35 kJ m^{-3} towards an out-of-plane anisotropy. If assumed that this variation comes from the Co/Gr interface, one can convert in interfacial anisotropy $\Delta K_S = 5 \times 10^{-2}$ mJ m^{-2} or around 30 μeV per Co atom. This is typically ten times smaller than expected from calculations for an ideal Co/Gr interface [9] and five times smaller than the experimental measurement with C_{60}/Co [7]. A likely explanation is that the interfacial hybridizations between C p_z orbitals and Co d_{z^2} orbitals are weaker in such samples than in samples realized on single crystal under ultrahigh vacuum

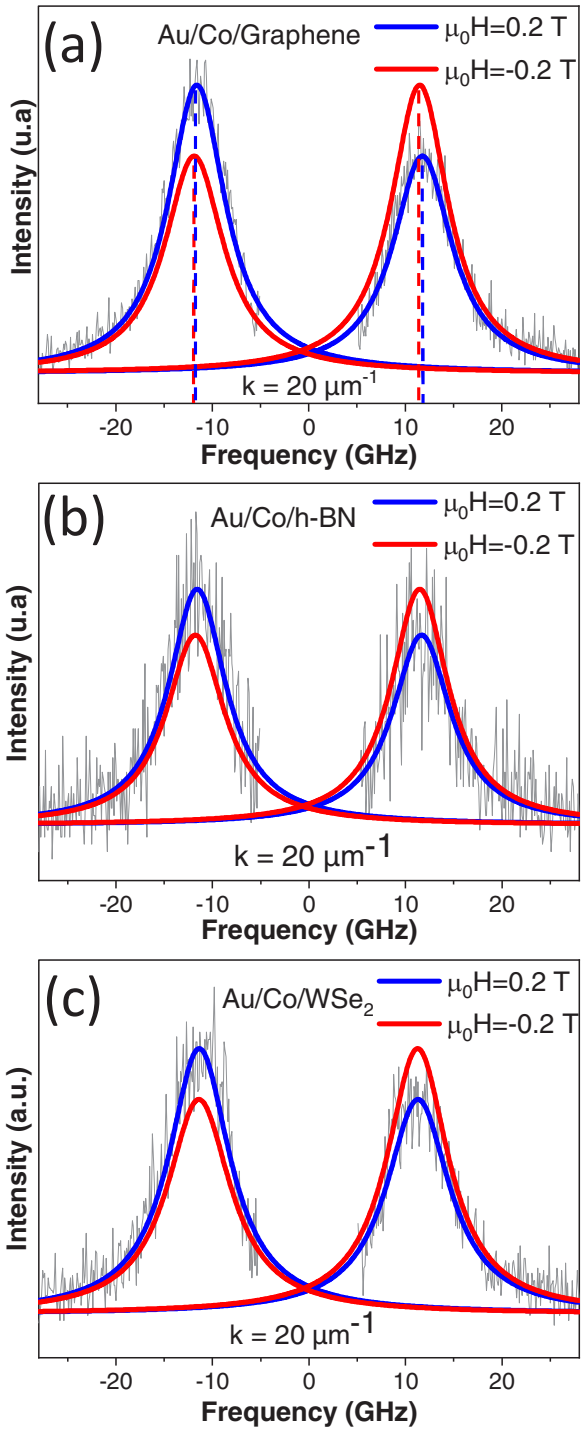

FIG. 5. BLS spectra for (a) Co/Gr, (b) Co/h-BN and (c) Co/WSe_2 systems. They were recorded for a wave number $k = 20\ \mu m^{-1}$ under applied magnetic fields H = 0.2 T and −0.2 T to evidence frequency difference between Stokes and anti-Stokes lines.

conditions. The first reason is that the surface energy of Co is far higher than the one of graphene, meaning that the growth is certainly occurring through three-dimensional clusters, randomly oriented, with numerous grain boundaries, giving rise to a poor quality of the interface. This picture is further confirmed by the important inhomogeneous broadening measured in Sec. III. A second reason is that in the clean room

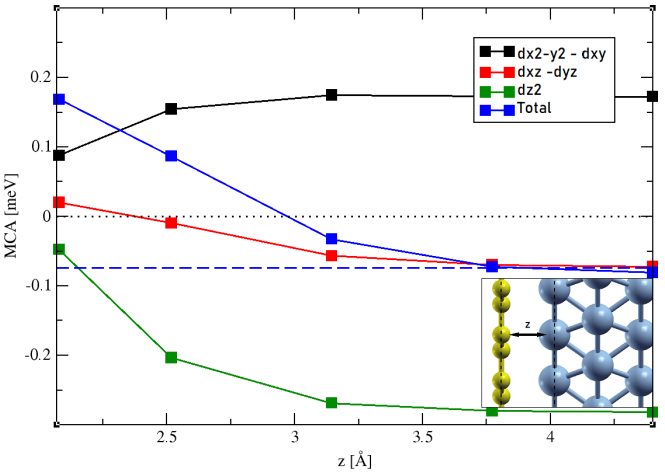

FIG. 6. MCA $= E_{\parallel} - E_{\perp}$ for the surface layer according to the distance between graphene and cobalt. In blue, the total MCA whose the limit is the free cobalt surface value in blue dashed line. The d orbitals contributions are shown in black, red and green, for respectively, the average between $d_{x^2-y^2}$ and d_{xy} orbitals, the average between d_{xz} and d_{yz} orbitals, and the d_{z^2} orbital.

process that is used in this study, the 2D materials are in contact with polymers and air before the Co deposition. It is therefore possible that a contamination layer induces again a poor quality of the interface. In order to better quantify how this loss of hybridization can affect the value of the interfacial anisotropy, we have performed calculations of the Co/graphene interface with a varying distance between both materials. The calculations are done using density functional theory (DFT) in the generalized gradient approximation approach and Perdew-Burke-Ernzerhof parametrization in plane waves, with `Quantum ESPRESSO` [30,31]. Pseudopotentials have been chosen to be ultrasoft, the basis size for plane waves is determined by the cutoff of 30 Ryd for the wave function, and 300 Ryd for the charge density. The magnetic anisotropy, and its local components, have been obtained by a three step process based on the magnetic force theorem [7,32,33] and a Marzari-Vanderbilt cold smearing with a broadening of 0.05 eV was used. 25 × 25 k points have been used for the self-consistent calculation (without SOC) and 50 × 50 k points for the non- self-consistent step including spin orbit. The thin film has been described with a sufficient vacuum thickness of 11 A in the z direction to avoid spurious periodic slabs-slab interactions. Since the graphene essentially hybridizes with the outermost surface layer of cobalt we have calculated the contribution of this layer to the total magnetic anisotropy using the procedure described in Ref. [32].

Figure 6 shows that the total anisotropy of the outermost cobalt layer is strongly affected by the distance between cobalt and graphene. Whereas the interfacial anisotropy (difference between the hybridized system and the free cobalt layer) reaches 0.25 meV per atom for the equilibrium distance between Co(0001) and graphene (2.1 Å), it drops by one order of magnitude at 3.1 Å. The decomposition on the different Co orbitals of this anisotropy is very instructive. Indeed, we can observe that d_{xz}-d_{yz} and d_{xy}-$d_{x^2-y^2}$ contributions to the magnetic anisotropy are not much affected by the presence

of graphene, while the d_{z^2} one, which favors strongly in-plane magnetization for bare Co, is almost vanishing in contact with graphene. This orbital selective quenching of the anisotropy leads to an overall interfacial anisotropy that has the same trend as the d_{z^2} contribution, with a fast decrease of the effect with the distance. Such a result could explain in our sample the small measured value of the anisotropy change at Co/Gr due to the presence of an interfacial corrugation which increases in average the distance between the graphene and Co layers. The origin of such a corrugation can be due to the highly polycristalline nature of the Co layer but also to buckling at the interface [34].

B. Dzyalonshinskii-Moriya interaction

The experimental results of Sec. III C show a small DMI value of 0.1 $mJ.m^{-2}$ that is roughly independant of the nature of the 2D material. In the case of cobalt/graphene, it can be compared with a recent experimental determination in Gr/Co/Ru of 0.16 meV/Co atom (around 0.2 mJ m^{-2}), that was basically explained in the framework of a Rashba model [14]. It is worth noting that a significant larger value (0.8 mJ m^{-2}) was deduced from domain wall motions in a graphene/Co/Pt(111) sample, although the role of Pt is certainly delicate to unravel [13]. In those last two cases, however, the graphene/Co interface is realized by intercalation of Co through the graphene layer, previously synthetized on either Ru or Pt. To our knowledge, only one recent paper has reported the direct growth of a ferromagnetic layer on graphene with a study of its magnetic properties and has found a small DMI of 0.07 mJ m^{-2} for a 3-nm $Fe_{20}Ni_{80}$ film, in rather good agreement with our determination [15]. Concerning h-BN and WSe_2 interfaces, it is surprising to find roughly the same DMI value that can hardly be ascribed to a Rashba effect. Further experimental and theoretical investigations will be needed to better understand the origin of DMI at such interfaces.

V. CONCLUSION

We have investigated by using a BLS technique the perpendicular magnetic anisotropy, the magnetic damping and the DMI in a thin cobalt Co layer deposited on graphene, h-BN, and WSe_2 flakes in a devicelike configuration. We have observed a small enhancement of the perpendicular magnetic anisotropy in presence of the 2D material, although less than expected from a theoretical point of view. We ascribe this behavior to a disordered interface, as confirmed by an increased magnetic damping. Moreover, DFT calculations show that the distance between Co and C atoms is a key parameter, with the interfacial magnetic anisotropy decreasing by one order of magnitude when the distance increases by 1 Å. A weak DMI is also measured on the three 2D materials, which is lower in the case of Co/graphene than in single crystal samples with the magnetic layer grown by intercalation below the graphene layer. Those results mainly show that when using such a clean room process for the deposition of a Co layer on 2D materials, the magnetic properties are not strongly modified at the interface.

ACKNOWLEDGMENTS

This project has received funding from the European Union's Horizon 2020 research and innovation programme under Grant agreement No. [766726]. C.B. and J.R. acknowledge financial support from the Ville de Paris Emergence program (2DSPIN project) and from the Région Ile-de-France in the framework of DIM Nano-K through the research project "Spin transport at the Molecular Scale". Y.R. and S.M.C. acknowledge financial support from the Région Ile-de-France (convention 1763) through the DIM Nano-K (BIDUL project).

[1] K. S. Novoselov, A. Mishchenko, A. Carvalho, and A. H. Castro Neto, Science **353**, aac9439 (2016).
[2] B. Dlubak, M.-B. Martin, C. Deranlot, B. Servet, S. Xavier, R. Mattana, M. Sprinkle, C. Berger, W. A. D. Heer, F. Petroff, A. Anane, P. Seneor, and A. Fert, Nat. Phys. **8**, 557 (2012).
[3] W. Han, R. K. Kawakami, M. Gmitra, and J. Fabian, Nat. Nanotechnol. **9**, 794 (2014).
[4] J. Wang, X. Xu, X. Mu, F. Ma, and M. Sun, Materials Today Physics **3**, 93 (2017).
[5] J. A. Reyes-Retana and F. Cervantes-Sodi, Sci. Rep. **6**, 24093 (2016).
[6] H. Yuan, X. Wang, B. Lian, H. Zhang, X. Fang, B. Shen, G. Xu, Y. Xu, S.-C. Zhang, H. Y. Hwang, and Y. Cui, Nat. Nanotechnol. **9**, 851 (2014).
[7] K. Bairagi, A. Bellec, V. Repain, C. Chacon, Y. Girard, Y. Garreau, J. Lagoute, S. Rousset, R. Breitwieser, Y.-C. Hu, Y. C. Chao, W. W. Pai, D. Li, A. Smogunov, and C. Barreteau, Phys. Rev. Lett. **114**, 247203 (2015).
[8] N. Rougemaille, A. T. N'Diaye, J. Coraux, C. Vo-Van, O. Fruchart, and A. K. Schmid, Appl. Phys. Lett. **101**, 142403 (2012).
[9] H. Yang, A. D. Vu, A. Hallal, N. Rougemaille, J. Coraux, G. Chen, A. K. Schmid, and M. Chshiev, Nano Lett. **16**, 145 (2016).
[10] A. D. Vu, J. Coraux, G. Chen, A. T. N'Diaye, A. K. Schmid, and N. Rougemaille, Sci. Rep. **6**, 24783 (2016).
[11] K. Bairagi, A. Bellec, V. Repain, C. Fourmental, C. Chacon, Y. Girard, J. Lagoute, S. Rousset, L. Le Laurent, A. Smogunov, and C. Barreteau, Phys. Rev. B **98**, 085432 (2018).
[12] D. Odkhuu, T. Tsevelmaa, P. Taivansaikhan, N. Park, S. C. Hong, and S. H. Rhim, Phys. Rev. B **99**, 014419 (2019).
[13] F. Ajejas, A. Gudn, R. Guerrero, A. Anadn Barcelona, J. M. Diez, L. de Melo Costa, P. Olleros, M. A. Nio, S. Pizzini, J. Vogel, M. Valvidares, P. Gargiani, M. Cabero, M. Varela, J. Camarero, R. Miranda, and P. Perna, Nano Lett. **18**, 5364 (2018).
[14] H. Yang, G. Chen, A. A. C. Cotta, A. T. N'Diaye, S. A. Nikolaev, E. A. Soares, W. A. A. Macedo, K. Liu, A. K. Schmid, A. Fert, and M. Chshiev, Nat. Mater. **17**, 605 (2018).
[15] A. K. Chaurasiya, A. Kumar, R. Gupta, S. Chaudhary, P. K. Muduli, and A. Barman, Phys. Rev. B **99**, 035402 (2019).

[16] A. Hrabec, M. Belmeguenai, A. Stashkevich, S. M. Chérif, S. Rohart, Y. Roussigné, and A. Thiaville, Appl. Phys. Lett. **110**, 242402 (2017).
[17] H. Li, J. Wu, X. Huang, G. Lu, J. Yang, X. Lu, Q. Xiong, and H. Zhang, ACS Nano **7**, 10344 (2013).
[18] M. M. Benameur, B. Radisavljevic, J. S. Hron, S. Sahoo, H. Berger, and A. Kis, Nanotechnology **22**, 125706 (2011).
[19] F. Pizzocchero, L. Gammelgaard, B. S. Jessen, J. M. Caridad, L. Wang, J. Hone, P. Bøggild, and T. J. Booth, Nat. Commun. **7**, 11894 (2016).
[20] X. Ma, G. Yu, C. Tang, X. Li, C. He, J. Shi, K. L. Wang, and X. Li, Phys. Rev. Lett. **120**, 157204 (2018).
[21] See Supplemental Material at http://link.aps.org/supplemental/10.1103/PhysRevMaterials.5.014004 for experimental details describing how to set accurately the zero frequency shift position; the model of calculation of the spin waves frequency and the full width at half maximum of the Brillouin lines.
[22] P. J. Metaxas, J. P. Jamet, A. Mougin, M. Cormier, J. Ferré, V. Baltz, B. Rodmacq, B. Dieny, and R. L. Stamps, Phys. Rev. Lett. **99**, 217208 (2007).
[23] M. Belmeguenai, J.-P. Adam, Y. Roussigné, S. Eimer, T. Devolder, J.-V. Kim, S. M. Chérif, A. Stashkevich, and A. Thiaville, Phys. Rev. B **91**, 180405 (2015).
[24] C. Chappert and P. Bruno, J. Appl. Phys. **64**, 5736 (1988).
[25] H. Bouloussa, R. Ramaswamy, Y. Roussigné, A. Stashkevich, H. Yang, M. Belmeguenai, and S. M. Chérif, J. Phys. D **52**, 055001 (2018).
[26] M. Belmeguenai, H. Tuzcuoglu, M. S. Gabor, T. Petrisor, C. Tiusan, D. Berling, F. Zighem, T. Chauveau, S. M. Chérif, and P. Moch, Phys. Rev. B **87**, 184431 (2013).
[27] M. Toka, S. Bunyaev, G. Kakazei, D. Schmool, D. Atkinson, and A. Hindmarch, Phys. Rev. Lett. **115**, 056601 (2015).
[28] J.-H. Moon, S.-M. Seo, K.-J. Lee, K.-W. Kim, J. Ryu, H.-W. Lee, R. D. McMichael, and M. D. Stiles, Phys. Rev. B **88**, 184404 (2013).
[29] H. Bouloussa, J. Yu, Y. Roussigné, M. Belmeguenai, A. Stashkevitch, H. Yang, and S. M. Chérif, J. Phys. D **51**, 225005 (2018).
[30] P. Giannozzi, S. Baroni, N. Bonini, M. Calandra, R. Car, C. Cavazzoni, D. Ceresoli, G. L. Chiarotti, M. Cococcioni, I. Dabo, A. Dal Corso, S. de Gironcoli, S. Fabri, G. Fratesi, R. Gebauer, U. Gerstmann, C. Gougoussis, A. Kokalj, M. Lazzeri, L. Martin-Samos, N. Marzazi, F. Mauri, R. Mazzarello, S. Paolini, A. Pasquarello, L. Paulatto, S. Sbraccia, C. Scandolo, G. Sclauzero, A. P. Seitsonen, A. Smogunov, P. Umari, and R. M. Wentzcovitch, J. Phys.: Condens. Matter **21**, 395502 (2009).
[31] P. Giannozzi, O. Andreussi, T. Brumme, O. Bunau, M. Buongiorno Nardelli, M. Calandra, R. Car, C. Cavazzoni, D. Ceresoli, M. Cococcioni, N. Colonna, I. Carnimeo, A. Dal Corso, S. de Gironcoli, P. Delugas, R. A. DiStasio Jr., A. Ferretti, A. Floris, G. Fratesi, G. Fugallo, R. Gebauer, U. Gerstmann, F. Giustino, T. Gorni, J. Jia, M. Kawamura, H.-Y. Ko, A. Kokalj, E. Kkbenli, M. Lazzeri, M. Marsili, N. Marzari, F. Mauri, N. L. Nguyen, H.-V. Nguyen, A. Otero-de-la Roza, L. Paulatto, S. Ponc, D. Rocca, R. Sabatini, B. Santra, M. Schlipf, A. P. Seitsonen, A. Smogunov, I. Timrov, T. Thonhauser, P. Umari, N. Vast, X. Wu, and S. Baroni, J. Phys.: Condens. Matter **29**, 465901 (2017).
[32] D. Li, A. Smogunov, C. Barreteau, F. Ducastelle, and D. Spanjaard, Phys. Rev. B **88**, 214413 (2013).
[33] L. Le Laurent, C. Barreteau, and T. Markussen, Phys. Rev. B **100**, 174426 (2019).
[34] E. Voloshina and Y. Dedkov, Phys. Rev. B **93**, 235418 (2016).